Available online at www.sciencedirect.com
SCIENCE DIRECT®
ELSEVIER
Journal of Magnetism and Magnetic Materials 284 (2004) 239–252
Journal of magnetism and magnetic materials
www.elsevier.com/locate/jmmm

Effect of Cr substitution on transport and magnetic ordering in $Nd_{0.50}Sr_{0.50}Mn_{1-x}Cr_xO_3$ ($0.001 \leqslant x \leqslant 0.20$)

C.M. Srivastava[a], R.K. Dwivedi[b], Saket Asthana[b], A.K. Nigam[c], D. Bahadur[b,*]

[a] *Department of Physics, Indian Institute of Technology, Mumbai 400076, India*
[b] *Department of Metallurgical Engineering and Materials Science, Indian Institute of Technology, Mumbai 400076, India*
[c] *Tata Institute of Fundamental Research, Homi Bhabha Road, Mumbai 400005, India*

Received 19 February 2004; received in revised form 18 June 2004
Available online 21 July 2004

Abstract

Chromium substitution in the charge ordered compound $Nd_{0.50}Sr_{0.50}MnO_3$ has been studied within the concentration range of 20% to examine its effect on magnetic and transport properties. It is found that the system comprises of three distinct magnetic phases whose percentage depends on the chromium concentration, the temperature and the external magnetic field. As the system is cooled, it changes from paramagnetic insulating type to a predominantly ferromagnetic metal (FM) and finally to a dominating anti-ferromagnetic insulating phase with A, CE or C-type of order depending on the chromium concentration. The appearance of three symmetrical loops in the hysteresis curve of M vs. H at 5 K for $x = 0.01$ indicates the simultaneous presence of C, A and FM type phases in the system.
© 2004 Elsevier B.V. All rights reserved.

PACS: 75.47.Lx

Keywords: Manganites; Charge ordering; Magnetic; Perovskite

1. Introduction

In recent years several attempts have been made to describe the complex correlation between the magnetic and transport properties of the manganate perovskite $(R_{1-x}M_x)MnO_3$ (R = Nd, Pr, Sm, M = Ca, Sr) generally in terms of the competition between the double exchange and superexchange [1–10]. Of special interest in this series have been the half-doped manganites such as $Nd_{0.5}Sr_{0.5}MnO_3$ and $Pr_{0.5}Sr_{0.5}MnO_3$ which are at the threshold of the ferromagnetic to antiferromagnetic phase transition. Further, at low temperatures, they comprise of regions with three different microscopic magnetic phases and two crystallographic structures coexisting. These are a

*Corresponding author. Tel.: +91222576-7632; fax: +91222576-3480.
E-mail address: dhiren@met.iitb.ac.in (D. Bahadur).

0304-8853/$ - see front matter © 2004 Elsevier B.V. All rights reserved.
doi:10.1016/j.jmmm.2004.06.042

ferromagnetic (FM) metallic phase with orthorhombic (Imma) structure, an antiferromagnetic (AFM) phase with A-type spin order, an orthorhombic (Imma) structure and an AFM-CE type spin order with monoclinic ($P2_1/m$) structure [6]. The volume fraction of these three magnetic phases in $Nd_{0.5}Sr_{0.5}MnO_3$ at any given temperature determined through neutron scattering is found to depend on the presence of the external magnetic field, H_0. It is found that in the presence of H_0, the FM phase is most stable while AFM-CE is least stable, so the region of the FM phase grows at the expense of the regions with AFM-CE and AFM-A phases when the sample is subjected to H_0 [8]. With $H_0 \sim 1$ A/m the magnetic energy per Mn atom is of the order of 0.1 meV, the instability of the CE- and A- magnetic phases is a quantum mechanical phenomenon not fully understood. It is however believed that a very delicate competition exists between the three phases near the Mn^{4+}: Mn^{3+} ratio of unity and small changes in this ratio stabilizes one phase over the other. For example, the FM phase in NSMO is stabilized when Mn^{4+}: $Mn^{3+} < 1$ and AFM-A phase is stabilized for Mn^{4+}: $Mn^{3+} > 1$. On the other hand, the coulomb stabilization associated with long-range and orbital ordering is essential for the stability of the AFM-CE state and hence it is observed only in the vicinity of the Mn^{4+}: $Mn^{3+} = 1$. Kajimoto et al. [6] have studied the hole-concentration-induced transformation of the magnetic and orbital structures in $Nd_{1-y}Sr_yMnO_3$ ($0.49 \leqslant y \leqslant 0.75$) using neutron diffraction measurements on melt grown polycrystalline sample. They observe a systematic transformation of the crystalline and magnetic structures and find that as y is increased from 0.49 the system exhibits an evoluation from the metallic ferromagnet state to a metallic A-type AFM state and then to an insulating C-type AFM state when y exceeds 0.6. The CE-type charge ordered AFM state is observed only in the vicinity of $y = \frac{1}{2}$ and it coexists with the A-type AFM state for $y \geqslant \frac{1}{2}$ indicating that the energy difference between these two states is very small. We have carried out the hole-concentration-induced changes in the magnetic and transport properties of $Nd_{0.5}Sr_{0.5}Mn_{1-x}Cr_xO_3$ ($0.001 \leqslant x \leqslant 0.2$). We show that chromium doping in the half-doped manganite $Nd_{0.5}Sr_{0.5}MnO_3$ changes the hole-concentration on lines similar to that produced by the change in strontium concentration in $Nd_{1-y}Sr_yMnO_3$. A detailed discussion of the phase diagram of $Nd_{1-y}Sr_yMnO_3$($0.49 \leqslant y \leqslant 0.75$) by Kajimoto et al. [6] has shown that (i) the insulating CE-type ordering is observed only in a very narrow range near $y \sim 0.50$ and coexists with metallic FM type spin order for $y < 0.5$ and the A-type AFM order for $y > 0.50$, (ii) in the metallic A-type AFM phase the lattice spacing in the direction of the AFM stacking is the smallest, indicating strong evidence of the $d(x^2 - y^2)$-type ordering within the FM layers, (iii) for $y > 0.60$ the magnetic order changes from A-AFM to C-AFM type, (iv) for $y = 0.49$ when CE spin order dominates the behaviour of resistivity in the $T < T_N$ region, is very different compared to $y = 0.51$ when the A-type AFM order coexists along with the CE-order. Lorentz microscopy studies have revealed that the micro domains of different magnetic order in such systems are of 20–30 nm in size [9]. For $y = 0.49$ a sharp increase in resistivity occurs below T_N due to the CE-type charge order till about 100 K and then the increase ceases due to the presence of the FM order with moment of $0.8\,\mu_B$ that coexists with the CE-type AFM spin order. On the other hand, for $x = 0.51$ below T_N a modest increase in resistivity occurs due to the onset of the A-type AFM spin order and then a second almost linear increase in resistivity occurs below $T_N^{CE} < T_N$ due to the onset of CE-type charge order whose volume fraction increases as the temperature is decreased.

The present system $Nd_{0.5}Sr_{0.5}Mn_{1-x}Cr_xO_3$ (NSMCO) coincides with $Nd_{1-y}Sr_yMnO_3$ (NSMO) at $x = 0$, $y = 0.5$. In the former, increasing x varies the hole-concentration in much the same way as increasing y beyond 0.5 in the latter, specially for small increments in x and y. There are however significant differences that arise due to difference in the radii of Cr^{3+}(0.615 Å) and Sr^{2+}(1.44 Å) ions. The substitution of Mn^{3+}(0.645 Å) with smaller Cr^{3+} does not affect the crystal structure in NSMCO while increase in strontium concentration in NSMO affects the crystal structure [6]. Further, this affects the

tolerance factor, t, defined as $t = r_{A-O}/\sqrt{2}r_{B-O}$ with r_{A-O} and r_{B-O} being the average A-cation–oxygen and B-cation–oxygen distances, respectively, and plays a dominant role in defining the boundaries of the phase diagram. For $0 \leqslant x \leqslant 0.2$, '$t$' changes from 0.9803 to 0.9835 in NSMCO while for $0.5 \leqslant x \leqslant 0.6$ it changes from 0.9803 to 0.9921 in NSMO. The other difference arises from the magnetic moment of $Cr^{3+}(t_{2g}^3 e_g^0)$ which is isoelectronic with Mn^{4+} and so it participates in the superexchange interaction with Mn^{3+} and Mn^{4+} ions but not in the double exchange interaction. We discuss the phase diagram of NSMCO in Section 4.

The magnetic and transport behaviour of the hole-doped mangnates arising from the competition between the ferromagnetic double exchange and antiferromagnetic superexchange can be analyzed on the basis of de Gennes approach [11]. Here T_c and T_N are expressed in terms of energies due to superexchange interaction and are compared with the contribution from the double exchange in terms of the gain in energy due to delocalization. This is discussed in Section 4.

The coupling of the charge carriers to the longitudinal phonons arising from the mixed valency of the Mn ions is discussed in Section 3. In this case the charge carriers behave as small polarons and in the correlated polaron model developed by one of the authors [12] expressions for the resistivity of the compound is obtained for both the FM and the AFM-spin states. This model explains the abrupt rise in resistivity at T_N and the widely dissimilar behaviour of $\rho(T)$ curves within the metallic FM and the AFM-CE phases. The model also accounts for the change in shape of the $\rho(T)$ curve for $x > 0.005$ where the abrupt increase in resistivity at T_N disappears and a continuous increase in resistivity is observed as T decreases. It is known that the system comprises of different regions of magnetic and crystallographic phases whose volume fraction depends on temperature and the external magnetic field. Because of the presence of multiphase regions the saturation moment M_0 determined by the extrapolation of the $M(H)$ curves from the ferromagnetic state to the zero field at low temperatures does not often reach the average value of Mn-ion moment of $3.5\,\mu_B$. It is only recently that Hayashi et al. [13] have shown (using pulsed magnetic field upto 45 T) that the moment in $Pr_{0.45}Sr_{0.55}MnO_3$ has the value $3.4 \pm 0.1\,\mu_B$/f.u. We have studied M–H curves for $Nd_{0.5}Sr_{0.5}Mn_{0.99}Cr_{0.01}O_3$ at 5, 50 and 150 K between ± 6 A/m. This is discussed in Section 6.

The variation of magnetization with temperature for two different values of H_0, 0.5 and 5 A/m, for 1% Cr doping has been accounted assuming that the system consists of two phases at the low field and a single phase at the high field. This is discussed in Section 5.

2. Experimental

Polycrystalline samples with compositions $Nd_{0.5}Sr_{0.5}Mn_{1-x}Cr_xO_3$ ($x = 0.001$, 0.005, 0.01, 0.05, 0.10, 0.15 and 0.20) have been prepared by conventional solid state reaction route. Appropriate amounts of Nd_2O_3, $SrCO_3$, MnO_2 and CrO_2 each of purity greater than 99.9%, were mixed for 6 h using acetone as a mixing media. The powder of each composition was ground and heated at 900 °C for 24 h with intermediate grinding. These powders were pelletized in the form of rectangular bars and heated at 1200 °C for 12 h. Final sintering was done at 1450 °C. Single-phase formation was confirmed by recording X-ray diffraction patterns of these compositions using Phillips PW1710 diffractometer. All the compositions have shown single-phase solid solution with orthorhombic structure. Resistivity measurement was done from 300–10 K using standard four probe method with the help of Keithley Nanovoltmeter (Type 181), Keithly Autotuning Programmable Current Source (Type 224) using Lakeshore close cycle system (CTI, Cryogenics, Helix Technology Corporation) and Temperature Controller (Type 330). Magnetic measurements have also been carried out using vibrating sample magnetometer (Oxford Maglab VSM) in a magnetic field of 0.5 A/m and in the temperature range of 5–300 K.

3. Nature of the charge carrier and transport

The transport properties of a system like $Nd_{0.5}Sr_{0.5}MnO_3$, which undergoes two magnetic

phase transformations at T_c and T_N as it is cooled from 300 K to low temperatures, are complex and a full understanding of these is lacking. The existence of mixed cation valence M^n, M^{n+1} on crystallographically equivalent sites permits electronic conduction through a dynamic ordering correlation of equal number of these ions on alternate sites. In this case the Verwey transition in magnetite [14] and the structural transitions in $Nd_{0.5}Sr_{0.5}MnO_3$ followed by decrease in electrical resistivity of several orders of magnitude are similar. Detailed studies by Ritter et al. [7] show that in NSMO both the FM and AFM-A phases that exist above $T_N(\sim 150\,K)$ have orthorhombic (Imma) symmetry but exhibit different cell constants. Below T_N a charge ordered phase with AFM-CE symmetry develops with a monoclinic ($P2_1/m$) structure and leads to a drop in volume thermal expansion $\Delta V/V$. This phase coexists with the FM and AFM-A phases down to 15 K with the volume fractions of each of the three phases changing rapidly with temperature and the applied magnetic field. In both cases in the metallic phase the electrons are coupled to an optical mode of the lattice through the dynamic Jahn–Teller effect. The ordering of the mobile electrons into sites made inequivalent by a Jahn–Teller lattice distortion leads to a structure with a lower symmetry space group accompanied by a metal to insulator transition [15].

In Fig. 1 we show the temperature dependence of resistivity of $Nd_{0.5}Sr_{0.5}Mn_{1-x}Cr_xO_3$-$(0.001 \leqslant x \leqslant 0.20)$. It may be noted that for $x = 0.001$ and 0.005, the system shows a sharp metal to insulator transition at $T_N \sim 150$ K. This is similar to that for a single crystal of $Nd_{0.5}Sr_{0.5}MnO_3(x = 0)$ [2]. By contrast for $0.005 < x \leqslant 0.15$, $\rho(T)$ shows no abrupt change between 10 and 300 K and the resistivity difference, $\rho(10\,K) - \rho(300\,K)$ is small. For $x = 0.2$ the resistivity shows monotonic increase in resistivity as the temperature is lowered.

It is discussed by Goodenough that in magnetite in the metallic region for $T > T_V$, the Verwey temperature, the charge carriers follow the Einstein diffusion equation for mobility and the number density with carriers treated as polarons is given by the random-walk approximation [15].

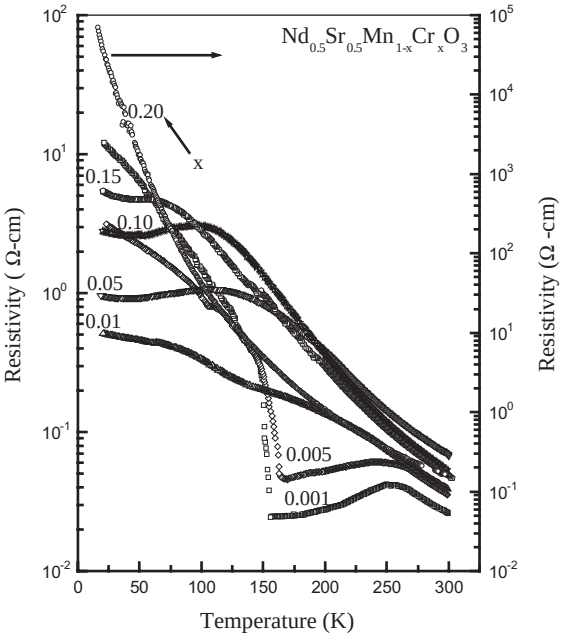

Fig. 1. The $\rho(T)$ curves for $Nd_{0.5}Sr_{0.5}Mn_{1-x}Cr_xO_3$-$(0.005 \leqslant x \leqslant 0.20)$. Note that the sharp metal to insulator transition near $T_N \sim 155$ K seen for $x = 0.001$ and 0.005 disappears for $x \geqslant 0.01$. Further, the nature of the $\rho(T)$ curves changes when x exceeds 0.15.

The resistivity can then be expressed as

$$\rho_F = \frac{AT}{n}\cosh^2(\varepsilon_p\beta/2)\exp(U\beta), \tag{1}$$

where n is the number density of mixed valence ions, ε_p is the small polaron stabilization energy associated with a dynamic correlation of Mn^{n+} and $Mn^{(n+1)+}$ ions and A is given by

$$A = \frac{1.13k_B}{D_0e^2}, D = D_0e^{-U\beta}, D_0 = a^2\nu_{ph}, \beta = 1/k_BT. \tag{2}$$

Here D is the Einstein diffusion coefficient, ν_{ph} is the frequency of the longitudinal optic phonon mode to which the electron is coupled and 'a' is the distance between the nearest neighbours of the mixed valence ions between which the hopping takes place with an activation energy, Srivastava [12] has considered the spin–spin (s–s) scattering along with the electron–phonon (e–p) scattering and taking $1/\tau_{s-s} = (1/\tau_{e-p})(1 - c^2m_s^2)\sigma_a^2$ and

$1/\tau_{\rm eff} = 1/\tau_{\rm e-p} + 1/\tau_{\rm s-s}$, the resistivity in the metallic phase can be expressed as

$$\rho_{\rm F} = \frac{AT}{n}[1 + (1 - c^2 m_{\rm s}^2(t))\sigma_{\rm a}^2]\cosh^2(\varepsilon_{\rm p}\beta/2)\exp(U\beta). \tag{3}$$

Here $m_{\rm s}(t) = M(T)/M(0)$ is the reduced magnetization at the reduced temperature $t = T/T_{\rm c}$, and is obtained for $s = \frac{1}{2}$, for which

$$m(t) = \tanh(m/t), \tag{3a}$$

$\sigma_{\rm a}$ is the short range charge order parameter

$$\sigma_{\rm a} = (1 - 0.75t_{\rm ca}^3)^{1/2} \quad t_{\rm ca} = T/T_{\rm ca} \tag{3b}$$

and U is given by

$$U = U_0 S_{\rm a}^2 \sigma_{\rm a}^2 (1 - cm(t))^2, \tag{4}$$

$$U_0 = \tfrac{1}{4}\langle n_{\rm ph}\rangle h\nu_{\rm ph}. \tag{5}$$

Here $S_{\rm a}$ is the long range order parameter, $T_{\rm ca}$ is the atomic order temperature and $n_{\rm ph}$ is the number of phonons in the polaron cloud round the charge carrier. For manganites we take $S_{\rm a} = 1$. For temperatures below $T_{\rm N}$ in the insulating phase, the scattering is dominated by the s–s scattering process and the diffusion process is suppressed, so the resistivity is given by

$$\rho_{\rm AF} = \frac{AT_{\rm N}}{n}\, m_{\rm s}^2(t')\cosh^2(\varepsilon_{\rm p}/2k_{\rm B}(T + \theta)). \tag{6}$$

Here A is the same as in Eq. (2) since the charge carriers jump from one site to another assisted by the phonon with activation energy, $U = 0$ and T is replaced by $T_{\rm N}$.

In Eq. (6) $m(t')$ is the reduced sublattice magnetization of the antiferromagnetically coupled lattices below $T_{\rm N} = T_{\rm CO}, m_{\rm s}(t') = M(T)/M(0)$, $0 < T < T_{\rm N}, t' = T/T_{\rm N}$. θ has been introduced along with T in Eq. (6) to take into account the zero point vibrations which prevent complete localization of the charge carriers as $T \to 0$. The relation in Eq. (6) is easily obtained assuming that the localization energy in the antiferromagnetic sublattices with neighbouring sites occupying opposite spins is given by $k_{\rm B}T_{\rm N}m_{\rm S}^2(t')$. The concentration of holes, $n(x)$ at x, is then $\exp(-{\rm e}Ex/k_{\rm B}T_{\rm N}m_{\rm s}^2(t'))$ where E is a constant electric field. The condition that in equilibrium no net current should flow is $\mu nE + D{\rm d}n/{\rm d}x = 0$, so $n(x)$ is proportional to $\exp(-\mu Ex/D)$. Now Eq. (6) follows since in the small polaron transport the charge carrier density is given by $n{\rm sech}^2\varepsilon_{\rm p}/2k_{\rm B}(T + \theta)$, where θ has been added for reasons discussed above [16].

We plot in Figs. 2(a) and (b) the resistivity curves for $x = 0$ and $x = 0.005$ respectively using Eq. (3) and Eq. (6). The experimental points for $x = 0$ sample is from Ref. [2] and is for a single crystal while for $x = 0.005$ in Fig. 2(b) is our result on a polycrystalline sample. The difference between Figs. 2(a) and (b) is similar to that found by Kajimoto et al. [6] for the resistivity of the FM sample with $y = 0.49$ and the AFM sample with $y = 0.51$ in $Nd_{1-y}Sr_yMnO_3$. They have accounted for the steep rise below $T_{\rm N}$ for $y = 0.49$ due to the CE-type charge order while the increase in $y = 0.51$ is attributed to the onset of the A-type AFM spin order and then a second increase at $T_{\rm N}^{\rm CE}$ due to the CE-type spin order whose volume fraction increases as the temperature is lowered. The $\rho(T)$ of the sample with $x = 0.005$ is similar in nature to the one with $y = 0.51$. The theoretical curve shown in Figs. 2(a) and (b) based on Eqs. (3) for the FM region between $T_{\rm N} < T < T_{\rm c}$ and Eq. (6) for the AFM region $10 < T < T_{\rm N}$ with the parameters given in Table 1 show that the correlated polaron model is able to account for the transport in both the Sr-doped and Cr-doped $Nd_{0.5}Sr_{0.5}MnO_3$ satisfactorily for small x and y close to $\frac{1}{2}$. We further conclude that Eq. (6) holds irrespective of the type of AFM spin order, A- or CE-, provided the parameters $A/n, \varepsilon_{\rm p}, \theta$ and c are appropriately chosen.

For $x > 0.005$ the abrupt change in $\rho(T)$ at $T_{\rm N}$ disappears (Fig. 1). The reason is that as temperature is decreased the paramagnetic phase changes to the AFM-A phase with the FM phase substantially suppressed. This is shown for $y > 0.5$ in $Nd_{1-y}Sr_yMnO_3$ through neutron scattering by Kajimoto et al. [6]. If the magnetic phase diagram is primarily determined by the ratio Mn^{4+}: Mn^{3+} a phase diagram can be obtained for NSMCO from that of NSMO on the basis that in the $Nd_{1-y}Sr_yMnO_3$ and $Nd_{0.5}Sr_{0.5}Mn_{1-x}Cr_xO_3$, this ratio is $y/1 - y$ and $0.5/(0.5 - x)$ respectively. As the two systems are the same at $y = 0.5$ and $x = 0$, for small values of y around 0.5 and $x = 0$

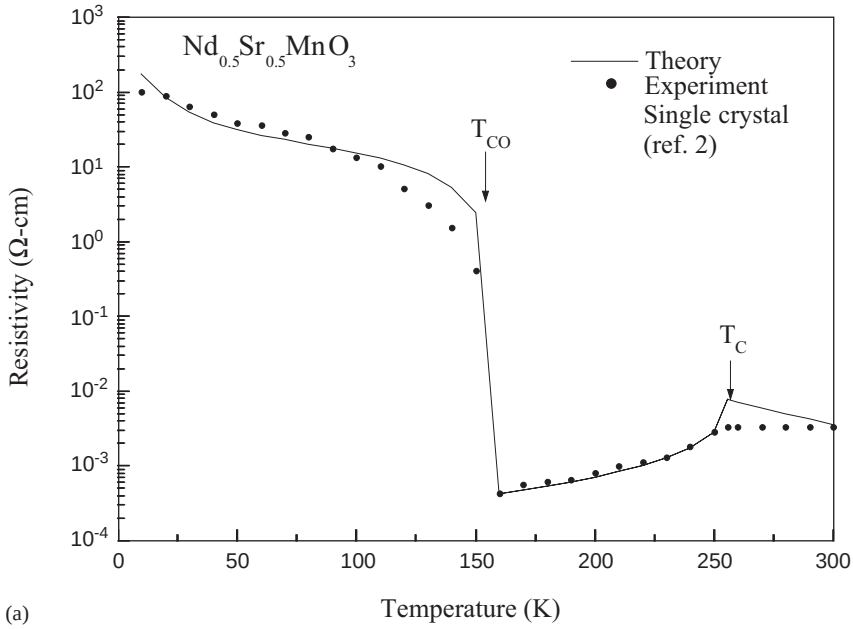

(a)

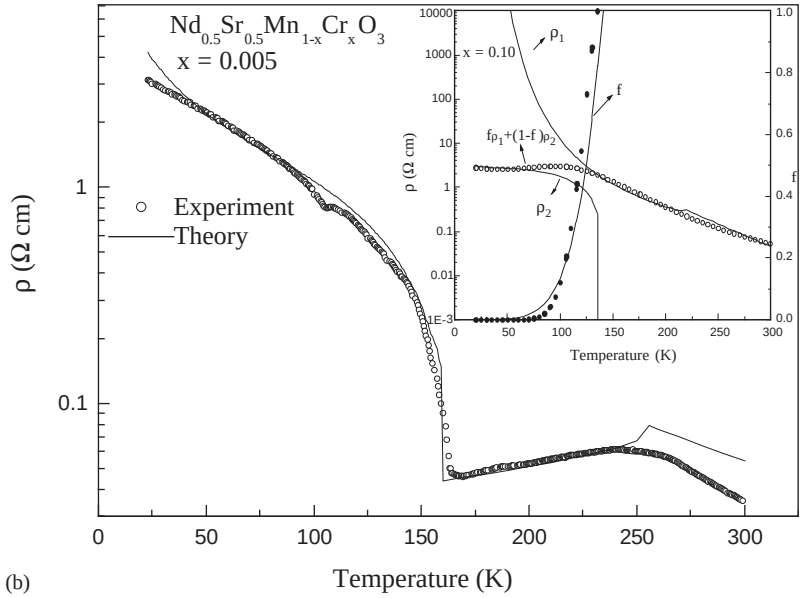

(b)

Fig. 2. (a) The $\rho(T)$ curve for single crystal $Nd_{0.5}Sr_{0.5}MnO_3$ calculated using Eq. (3) for the FM ($T_N < T < T_c$) and PM ($T_c < T \leqslant 300$ K) parts and parameters given in Table 1. For PM region, $m_s = 0$. Eq. (6) has been used to plot the $\rho(T)$ curve in the AFM ($T < T_N$) region. T_c is taken as 256 K and T_N as 158 K. The experimental points are from Kuwahara et al. [2] (b) The $\rho(T)$ curve for polycrystalline $Nd_{0.5}Sr_{0.5}Mn_{1-x}Cr_xO_3$ ($x = 0.005$ and 0.10 (inset)) calculated using Eqs. (3), (6) and (7) with parameters given in Table 1. Eq. (3) is used to fit the FM ($T_N < T < T_c$) and PM ($T_c < T \leqslant 300$ K) region with $m = 0$ for $x = 0.005$. Eq. (7) is used to fit $x = 0.10$ data in the inset. The volume fraction 'f' of the FM phase varies as $(T/T_N)^6$. For $x = 0$, $c = 1$ but for $x = 0.005$, $c = 0.5$. For $x = 0.10$, $c = 0.1$.

Table 1
Parameters used in fittings of the curves for the temperature variation of resistivity in $Nd_{0.5}Sr_{0.5}Mn_{1-x}Cr_xO_3(0.001 \leqslant x \leqslant 0.2)$ given in Fig. 1

x	T_c(K)	T_N(K)	$T_{N'}$(K)	Ferromagnetic				Antiferromagnetic					
				A/n (Ω cm K^{-1}) $\times 10^4$	n (10^{20}/cc)	ε_p (K)	U (K)	AT_N/N (Ω cm)	N (10^{17}/cc)	ε_p (K)	θ (K)	c	T_{ca} (K)
0.00[a]	256	158	—	0.018	325	130	806	14	6.6	130	20	1	350
0.001	256	156	—	0.40	14.6	130	400	0.8	114	130	45	0.5	350
0.005	246	165	—	0.80	7.31	130	400	0.75	129	280	60	0.5	350
0.01	250	175	27	0.26	23	130	600	0.46	222	30	20	0.1	350
0.05	220	140	37	0.60	10	130	600	0.60	136	30	20	0.1	350
0.10	220	140	37	0.33	17.7	130	900	2.60	31.5	30	20	0.1	320
0.15	200	140	37	0.25	25.4	130	900	4.19	20	30	20	0.1	330
0.20	200	150	25	0.17	34.4	130	700	7.0	12.5	150	10	0.05	330

For analysis of the curves Eq. (3) is used for the FM region ($T_N < T < T_c$). The value of A is obtained using Eq. (2) (see text) and $a_0 = 3.8329$ Å, $\nu_{ph} = 7 \times 10^{12}$ Hz. $\rho(T)$ in the paramagnetic phase is obtained from Eq. (3) with $m = 0$. Eq. (6) is used to fit $\rho(T)$ in the AFM region. For $x > 0.005$ $\rho(T)$ is fitted to Eq. (7). T_c and T_N are determined from the resistivity (Fig. 1) and $T_{N'}$ is obtained from the magnetization data (Fig 5). T_{ca} values are found to lie between 320 and 350 K.

[a]Single crystal.

the two systems should be similar in magnetic phases. The main difference that arises is due to the ionic radii of Sr^{2+}(1.44 Å) and Cr^{3+}(0.615 Å), so the tolerance factor changes as y and x increase as discussed earlier. Further the substitution of chromium leads to enhancement of the super-exchange interaction due to $Mn^{4+} - O^{2-} - Cr^{3+}$ linkages that replace $Mn^{4+} - O^{2-} - Mn^{3+}$ that promote double exchange. Kallel et al. [17] find that Cr doping in $La_{0.7}Sr_{0.3}Mn_{1-x}Cr_xO_3$ does not lead to any change in crystal structure for $0 \leqslant x \leqslant 0.5$ but leads to decrease in T_c which varies as a polynomial of degree two, $T_c = Ax^2 + bx + C$. This is justified on the basis of the model of exchange proposed by Anderson and Hasegawa [18]. In Section 4 we show that the expression for T_c and T_N that we obtain from de Genne's formulation [11] agrees with the experimental results on our system.

In the inset of Fig. 2(b) we have plotted the $\rho(T)$ curve for $x = 0.10$ and compared it with the theoretical curve obtained as follows:

$$\rho(T) = f\rho_1(T) + (1-f)\rho_2(T), \tag{7}$$

where $\rho_1(T)$ is the expression in Eq. (3) applies to the paramagnetic ($m = 0$) as well as the ferromagnetic ($m \neq 0$) region with spin–spin scattering significantly suppressed ($c = 0.1$) and with volume fraction f, and $\rho_2(T)$ is the expression in Eq. (6) and applies to the contribution from the volume fraction of the antiferromagnetic phase, $(1-f)$. A plot of f as a function of temperature is also given and shows that it varies as $(T/T_N)^6$ in the region $0 \leqslant T \leqslant T_N$. Similar fit to $\rho(T)$ is obtained for $0.01 \leqslant x \leqslant 0.15$ with the parameters given in Table 1.

From Table 1 we conclude the following:

(1) T_C and T_N are nearly the same for single crystal and polycrystalline samples for $0 \leqslant x \leqslant 0.005$ indicating that PM to FM and FM to AFM processes are intrinsic to the system.

(2) The upturn in $\rho(T)$ observed at low temperature in most of the $AMnO_3$(A = $Nd_{0.5}Sr_{0.5}$, $Pr_{0.5}Sr_{0.5}$) compounds is due to the number density varying as $\mathrm{sech}^2(\varepsilon_p/2k_B(T+\theta))$ and arises from the localization of the charge carriers in the antiferromagnetic region as $T \to 0$. For $0 \leqslant x \leqslant 0.005$ in Table 1, ε_p in the AFM phase is one order of magnitude larger than for $0.01 \leqslant x \leqslant 0.15$ and shows that for the former the magnetic order is mainly CE-type and for the latter it is A-type in the temperature region $0 \leqslant T \leqslant T_N$. The carrier density in the FM phase is nearly three orders of magnitude larger than in

the AFM phase. Further, the mobility is thermally activated in the FM phase while this is absent in the AFM phase. The difference in number density n and ε_p between the AFM-CE and AFM-A spin orders accounts for the four orders of magnitude smaller resistivity of $Pr_{1/2}Sr_{1/2}MnO_3$ at 5 K than the $Nd_{1/2}Sr_{1/2}MnO_3$ compound when the resistivity at T_N for both is nearly the same [19]. A calculation similar to above shows that in the AFM region for the Pr- and Nd- compounds the values of n are 3×10^{20}/cc and 6.6×10^{17}/cc and that of ε_p are 30 and 130 K respectively.

4. Magnetic phases

We treat the $Nd_{0.5}Sr_{0.5}Mn_{1-x}Cr_xO_3$ system in the molecular-field approximation of the ferromagnetic binary alloy. The magnetic unit cell in orthorhombically distorted perovskite has the dimensions $a \approx b \approx \sqrt{2}a_p$ and $c \approx 2a_p$ where a_p relates to the cubic perovskite [20]. We obtain $a_p \approx 3.8329$ Å for the present system for $x = 0$. Each magnetic unit cell contains 16 Mn atoms with Mn^{3+} and Mn^{4+} ions in equal numbers. The spins are collinear and constitute four sublattices each with a maximum of eight spins; $A_1(\uparrow), A_2(\uparrow)$, $B_1(\downarrow)$ and $B_2(\downarrow)$. The nearest neighbours of atoms on site 1 are on site 2 and vice versa [12]. The magnetic coupling is through double exchange (DE) and superexchange (SE). DE exists between unlike ions on A_1 and A_2 and B_1 and B_2 sublattices respectively. Amongst Mn^{3+} and Mn^{4+} ions DE favours FM coupling while SE favours A-, CE- and C- type AF coupling within and between successive planes in the c-direction. The spin arrangement for CE-, A- and C-type ordering is given in Ref. [6]. The spin ordering on the four sublattices for CE, A and FM-type order is shown in Fig. 3, where 3 and 4 in Fig. 3 indicate the Mn^{3+} and Mn^{4+} ions and the (±) indicate the spin direction in the *ab* plane which stack antiferromagnetically along the *c*-axis. In (a) the CE-type spin order is characterized by the alternate ordering of Mn^{3+} and Mn^{4+} ions and hence needs two octants to show the charge ordering . In A type of spin order the spins order ferromagnetically in the *ab* plane with the moments pointing along the *a*-axis and the planes are stacked antiferromagnetically along the *c*-axis. The C type

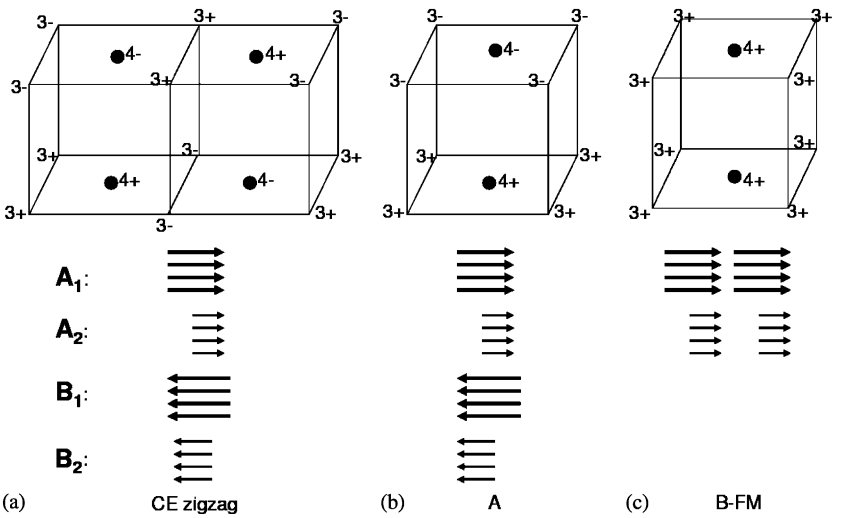

Fig. 3. The spin arrangement on an octant of a magnetic unit cell in $Nd_{0.5}Sr_{0.5}MnO_3$, (a) CE-type antiferromagnetism (b) A-type antiferromagnetism (c) FM-type ferromagnetism. The magnetic unit cell in orthorhombically distorted perovskite lattice has the dimensions, $a \approx b \approx \sqrt{2}a_p$ and $c \approx 2a_p$, where a_p relates to the cubic perovskite. We obtain $a_p = 3.8329$ Å. The magnetic unit cell contains 16 Mn atoms. The spin arrangement in the (a), (b) and (c)-type of magnetic order on the A_1, A_2, B_1, B_2 sublattices are shown with larger arrows representing $Mn^{3+}(4\mu_B)$ and smaller $Mn^{4+}(3\mu_B)$ ions. The (±) indicate the spin direction in the *ab* plane and three and four indicate the Mn^{3+} and Mn^{4+} ions.

is similar to Fig. 3(b) except that the spins order ferromagnetically along the c-direction while the neighbouring spins in the ab plane are in opposite direction. In Fig. 3(c) spins order ferromagnetically in the ab plane and the FM planes are stacked ferromagnetically along the c-axis. This is the spin order as described in Ref. [6] based on neutron scattering.

The dependence of magnetization on temperature can be described using a two sublattice model. In the FM phase for $x = 0$, eight spins each on sublattices A_1 and A_2 are ordered below T_c and as shown in Ref. [10], magnetization has a sharp transition at T_c. The expression for T_c obtained by deGenne [11] can be written as [12]

$$k_B T_c = \frac{2}{3}[z_a|J^a| - z_b|J^b| - z_c|J^c|]S^2 + \frac{2\xi z\varepsilon_p}{5}, \quad (8)$$

while in the insulating antiferromagnetic A-type spin arrangement , the Néel point is given by

$$k_B T_N = \frac{2}{3}[z_a|J^a| - z_b|J^b| + z_c|J^c|]S^2. \quad (9)$$

Here $z_i (i = a, b, c)$ are the number of nearest neighbours along the a, b, c directions, z is the total number of nearest neighbours, and J^i is the effective J in the i-direction and ξ is the number of charge carriers per Mn atom. Taking $J^a = 1.61$ meV, $J^b = J^c = 0.62$ meV similar to $La_{0.67}Ca_{0.33}MnO_3$ [12] and $\varepsilon_p = 130$ K, $\xi = 0.5$ in Eq. (8) we obtain $T_C = 256$ K as observed for $Nd_{0.5}Sr_{0.5}MnO_3$ (Table 1). In the AFM phase with $J^a = J^b = J^c = 0.62$ meV, T_N from Eq. (9) is 156 K close to the observed value (Table 1). The change from the FM phase to AF phase for $x = 0$ is due to the first order phase transformation from orthorhombic (Imma) to the monoclinic ($P2_1/m$) phase at T_N [7] where J^a changes from 1.61 to 0.62 meV with J^b and J^c remaining unchanged.

We are now able to show that there is a systematic change in the magnetic structure of $Nd_{0.5}Sr_{0.5}Mn_{1-x}Cr_xO_3$ as a function of the hole concentration x. For $x = 0$ the ground state spin order changes from PM to FM and then to CE-type antiferromagnet as the temperature is lowered. This is shown in Fig. 4. This change continues for $x = 0.001$ and 0.005. For $x > 0.005$ the sharp increase in resistivity at T_N disappears and a mixed phase FM + AFM-A appears below the phase FM as is evident from $\rho(T)$ data in Fig. 1 and $M(T)$ data in Fig. 5. A detailed analysis of these leads to a magnetic phase diagram for $Nd_{0.5}Sr_{0.5}Mn_{1-x}Cr_xO_3 (0 \leqslant x \leqslant 0.2)$ shown in Fig. 4. The presence of chromium leads to the nucleation of the AFM-C phase for $x > 0.005$. It is argued by Goodenough [15] that Cr^{3+} has preference for d^2sp^3 hybridization which would help d_{z^2} orbital formation of near neighbour Mn^{3+} ions leading to the AFM-C formation through superexchange. The crystal structure within this doping range probably does not change since the radii of Cr^{3+} and Mn^{3+} ions are nearly the same and the tolerance factor changes from 0.9803 at $x = 0$ to 0.9835 at $x = 0.2$. The abrupt change in ε_p at $x = 0.2$ appears to be an indication of change from AFM-A to AFM-C spin order. A continuous rise in resistivity with decrease in temperature observed for this composition is similar to that of $Nd_{1-y}Sr_yMnO_3$ with $y > 0.6$ where the spin order is AFM-C [6]

5. Field-induced magnetic phases

The low temperature phase near 125 K for $x = 0$ is found by Ritter et al. [7] to be phase segregated into two crystallographic structures, orthorhombic (Imma) A type AFM and FM magnetic phases and monoclinic ($P2_1/m$) with CE-type AFM phase. Under a field of 6 T the CE monoclinic phase completely transforms into the metallic ferromagnetic orthorhombic phase.

In Fig. 5 we give the plot of $M(T)$ for $0.005 \leqslant x \leqslant 0.20$ in the temperature range $5 \leqslant T < 300$ K obtained with $H = 0.5$ T. For $x = 0.005$ with sharp changes in the slope of the $\rho(T)$ curve we obtain $T_c = 246$ K and $T_N = 165$ K. This is given in Table 1. From Fig. 6 for $H = 0.5$ T the inflection point in the $M(T)$ curve gives $T_c = 256$ K and T_N, is obtained from the peak in the $M(T)$ curve and is 159 K. T_c and T_N values obtained at $H = 0.5$A/m from Fig. 5 are given in Table 2. These T_N values may be compared with those obtained from the $\rho(T)$ curves (Table 1).

It is shown in Ref. [6] that in A-type magnetic phase spins typically order ferromagnetically in the

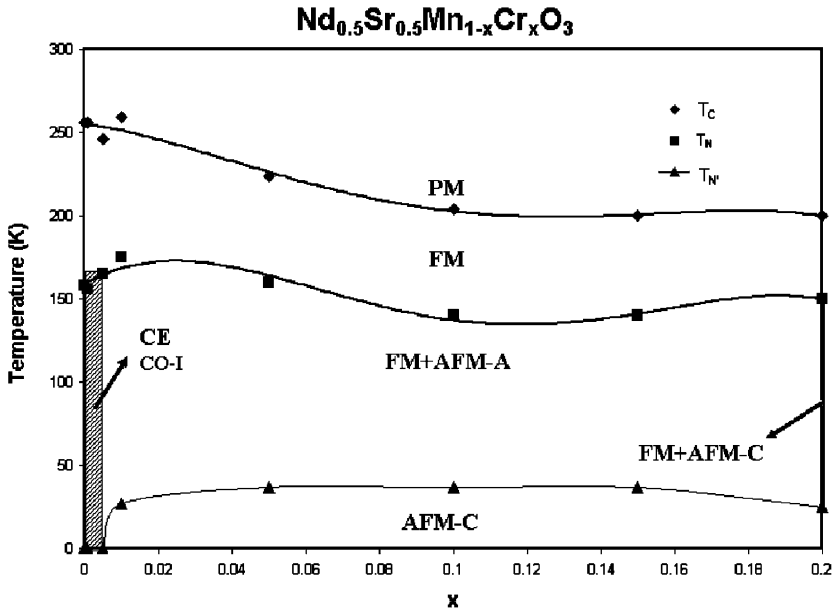

Fig. 4. The magnetic phase diagram of $Nd_{0.5}Sr_{0.5}MnO_3$ obtained by the $\rho(T)$ and $M(T)$ data in (Figs. 1 and 5). Each phase is denoted by a label; PM: paramagnetic insulator; FM: ferromagnetic metal; AFM: antiferromagnetic; CE: CE-type spin/charge order; A-A type spin order; C-C type spin order.

ab plane with the moments pointing towards the *a*-axis and the FM planes are stacked antiferromagnetically along the *c*-axis. We take that the sublattice magnetization in the molecular field approximation is given by spin $S=\frac{1}{2}$ since the magnetic order is a result of competition between the orbital, charge and spin ordering induced by the electron hopping processes in the doubly degenerate e_g orbital [10,11]. This is a crude approximation but since in this, local inhomogenities play an important role which is not fully understood. On this basis we can account for the broad features of this temperature and magnetic field driven transitions. Then the reduced magnetization, $m = M(T)/M(0)$ satisfies the relationship

$$m = \tanh(m/t), \tag{10}$$

where t is the reduced temperature $t = T/T_c$. The value $M(0) = N\mu$ is a function of the applied field, H, since even for very large fields exceeding 12 A/m, μ is less than the theoretical value of $3.5\,\mu_B$. It is only recently that Hayashi et al. [13] have achieved this value in a pulsed field of 45 A/m for $Pr_{0.45}Sr_{0.55}MnO_3$.

For the region $T_N < T < T_c$

$$m_1 = \tanh(m_1/t_1) \tag{11}$$

with $t_1 = T/T_c$.

In the region $0 < T < T_N$ in the presence of an external field, another FM region is stabilized whose magnetization is given by

$$m_2 = \tanh(m_2/t_2), \tag{12}$$

where $t_2 = T/T_N$. For the AFM volume region the effective reduced sublattice magnetization is given by

$$\bar{m} = m_1 - m_2. \tag{13}$$

Here $m_i = \mu_i(H,T)/\mu_i(H,0)(i=1,2)\mu_i(H,T)$ is the effective Bohr moment per formula unit at field H and temperature T. Eq. (13) follows as at T_N a fraction p of N spins change from FM spin arrangement to A-type spin arrangement forming antiferromagnetic sublattices and another FM spin system is stabilized whose temperature variation is given by Eq. (12). Since the response of the sublattices to the field H is to reduce the

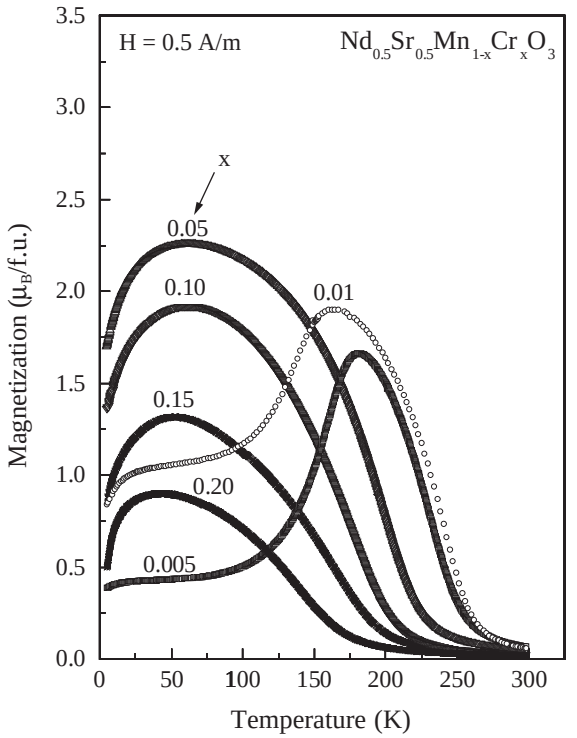

Fig. 5. Magnetization $M(T)$ curves for $0.005 \leqslant x \leqslant 0.20$ in $Nd_{0.5}Sr_{0.5}Mn_{1-x}Cr_xO_3$ at 0.5 A/m. T_c, T_N and $T_{N'}$ have been measured through the inflection point, maximum in the $M(T)$ curve and change in slope respectively and are given in Tables 1 and 2. Also given in Table 2 are the estimated values of $\mu_F(0)$ and $\mu_{AF}(0)$, the zero temperature magnetic moment per formula unit in the ferromagnetic (F) and antiferromagnetic (AF) phases obtained from these curves.

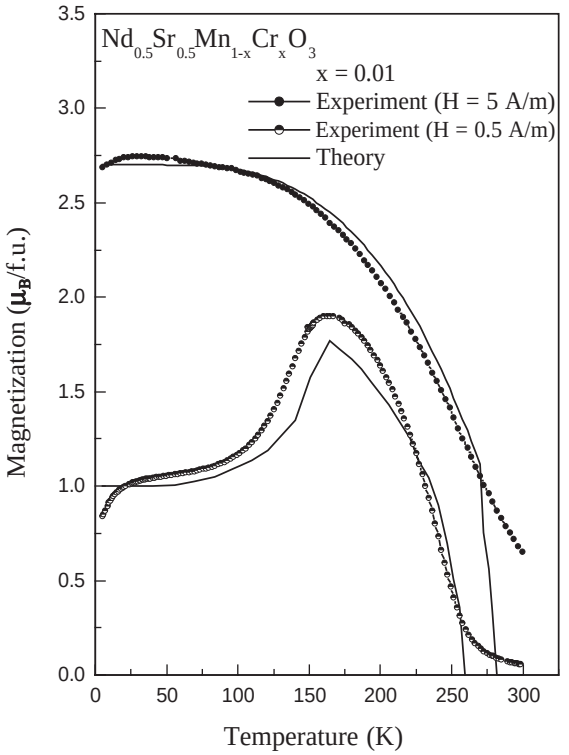

Fig. 6. Comparison of $M(T)$ plots for $H = 0.5$ and 5 A/m for $x = 0.01$ in $Nd_{0.5}Sr_{0.5}Mn_{1-x}Cr_xO_3$. At 5 A/m the transition from FM to AFM phase at T_N has disappeared. Further on increasing the field T_c shifts from 259 to 280 K. The theoretical plot using Eq. (11) with $\mu_F(0) = 2.70\,\mu_B$/f.u. and $T_c = 280$ K is compared with experiment and is in satisfactory agreement. The experimental curve for 0.5 A/m is compared with that obtained using Eq. (13) with the parameters given in Table 2.

magnetization of the FM sublattices, Eq. (13) follows.

In Fig. 6 we have given the plots of $M(T)$ at $H = 0.5$ and 5 A/m and compared it with theory using Eqs. (11) and (13). At 5 A/m, the FM to AFM transition disappears as also observed by Ritter et al. [7]. T_c is taken as 280 K and the value of $\mu_F(0)$ at $T = 0$ and $H = 5$ A/m is taken as $2.70\,\mu_B$. The fit to $M(T)$ data to Eq. (11) in Fig. 6 shows that the molecular-field approximation with $s = \frac{1}{2}$ is applicable. For the data at $H = 0.5$ A/m, $\bar{m}$ in Eq. (13) is obtained using $T_N = 155$ K and $\mu_{AF}(0) = 1.50\,\mu_B$. The difference in the behaviour of $M(T)$ curves near T_c for $H = 0.5$ and 5 A/m in Fig. 6 is due to fact that relatively low magnetic field induces transitions from the AFM-A state to FM metallic state as suggested by Kuwahara et al. [2].

We have analyzed the temperature variation of magnetization for $H = 0.5$ A/m shown in Fig. 5 on similar lines for $0.005 \leqslant x \leqslant 0.20$. The parameters obtained from the analysis are given in Table 2. The M–T curve indicates that the transition from paramagnetic (PM) to FM takes place at T_c and to FM + AFM-A regions takes place at T_N for $x \geqslant 0.005$. As the temperature is lowered the AFM-C spin state nucleates at $T_{N'}$. Near $T \to 0$ only AFM-C region exists for $0.01 < x < 0.2$ (Fig. 4). For $x \leqslant 0.01$, T_c and T_N are nearly constant but as x increases beyond 0.01, T_c and T_N both decrease (Table 1). In each case $T_{N,}$ obtained from zero field resistivity data in

Table 2
The parameters used to fit the $M(T)$ curves given in (Figs. 5 and 6) for $Nd_{0.5}Sr_{0.5}Mn_{1-x}Cr_xMnO_3(0.005 \leqslant x \leqslant 0.20)$ using Eqs. (11) and (13) (see text)

x	H(A/m)	T_c(K)	T_N	$T_{N'}$(K)	$\mu_F(0)$ (μ_B/f.u.)	$\mu_F(0)$ (μ_B/f.u.)
0.005	0.5	256	159	0	2.30	1.73
0.01	0.5	259	155	27	2.55	1.50
0.05	0.5	224	—	37	2.75	1.125
0.10	0.5	204	—	37	2.00	0.75
0.15	0.5	200	—	37	1.375	0.625
0.20	0.5	180	—	25	0.90	—
0.01	5	280	—	—	2.70	—

The zero-temperature magnetization in Bohr magneton per formula unit in the FM phase, $\mu_F(0)$, and in the AFM insulating phase, $\mu_{AF}(0)$, have been estimated from the $M(T)$ curves. T_c is estimated from the inflection point and T_N from the maximum in the $M(T)$ curve. $T_{N'}$ is obtained from the change in slope of $M(T)$ near $T \to 0$ and denotes the nucleation of the AFM-C phase.

Table 1 is higher, compared to the magnetization data at 0.5 A/m showing field induced metastability.

6. The *M–H* curve

For the $s = \frac{1}{2}$ model, the domain wall is thin as discussed by Zimmermann et al. [21]. Some information on the behaviour of domain wall in applied field can be obtained from the $M(H)$ plots as given for $Pr_{0.5}Ca_{0.5}Mn_{1-x}Cr_xMnO_3$ by Mahendrian et al. [22] and for $Nd_{0.5}Sr_{0.5}MnO_3$ in Ref. [4]. We have carried out these studies for $x = 0.01$ at 5, 50 and 150 K for applied field of $-6\,A/m \leqslant H \leqslant +6\,A/m$. These are shown in Figs. 7(a)–(c). The main features are: (i) presence of three nearly closed loops at 5 K, one symmetrically placed between ± 0.5 A/m around the origin, the other two lying between ± 0.5 and ± 6 A/m, (ii) at 5 K the virgin loop in the first quadrant is larger in area than the area of the subsequent loops while in the third quadrant these two loops are identical. This is similar to the $M–H$ loop in $Ce(Fe_{0.96}Al_{0.04})_2$ [23]. As the temperature is increased, the virgin and subsequent loops begin to merge but even at 150 K these can be distinguished, (iii) the moment per Mn atom at 6 A/m at 5 K for $x = 0.01$ is $2.78\,\mu_B$. These compare favourably with the observation of Mahendrian et al. [4] who reported a value of $1.3\,\mu_B$ for increasing H on the virgin curve and $2.8\,\mu_B$ for decreasing H for a sample with $x = 0$ at 50 K and at a field of 6 A/m. In the present case with simultaneous presence of CE and A-type-AF regions along with the FM-type ferromagnetic region the $M–H$ loop is affected as the coercivities of CE- and A- type regions are different from that of FM and C- type.

Amongst the four spin configuration (at $H = 0$), the states shown in Fig. 3 are probably such that on the application of a field CE-, A- and C- type change to FM-type. As the external field is applied the Zeeman energy, $-\mu H$, favours the growth of the FM-type spin configuration. The first loop near the origin shows the conversion of C- type to FM- type spin magnetic structures under the applied magnetic field. The first loop near the origin extends from $H = 0$ to $H = 0.1$ A/m at 5 K for $x = 0.01$, Fig. 7(a). Beyond 0.1 A/m the loop with hysteric behaviour probably originates from the conversion of A-type spin regions to FM-type under the influence of increasing Zeeman energy.

We conclude that at 5 K for $x = 0.01$, H_C is small (~ 1200 Oe) and remanence, M_r, is $\sim 1\,\mu_B$/f.u. and this accounts for the low field magnetic loop, which nearly disappears on heating to 50 K. This arises from C-type spin order (Fig. 4). On the other hand the high field loop has virgin loop larger than subsequent loops in the first quadrant even at 150 K. This arises from AFM-A type spin

Fig. 7. The magnetization vs. field plotted in (a) at 5 K for 0.01 for $Nd_{0.5}Sr_{0.5}Mn_{1-x}Cr_xO_3$. The three magnetic loops, one symmetrically placed round the origin and the other two high-field loops lying between $\pm 0.5\,A/m < H < \pm 6\,A/m$ in the first and third quadrant, show no saturation at 6 A/m. The cycling of the field on the high-field loop is shown by 1,2,3. (b) At 50 K, the low field loop has almost disappeared and the area of the high-field loops has decreased. (c) At 150 K, the low-field loop disappears and the high-field loop has decreased considerably but the difference between cycles one and three in the first quadrant is still noticeable.

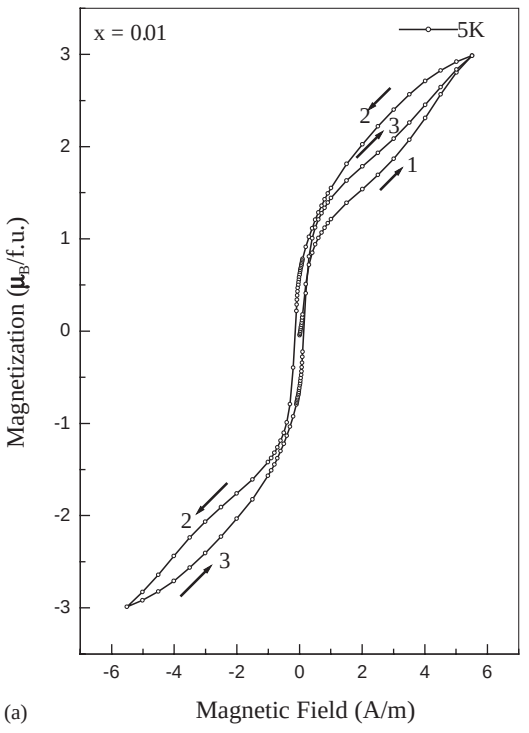
x = 0.01
5K
Magnetization (μB/f.u.)
Magnetic Field (A/m)
1
2
3
2
3

(a)

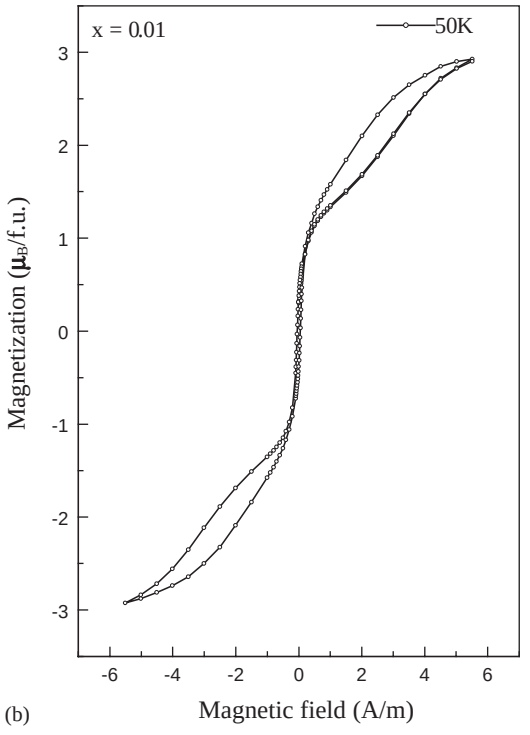
x = 0.01
50K
Magnetization (μB/f.u.)
Magnetic field (A/m)

(b)

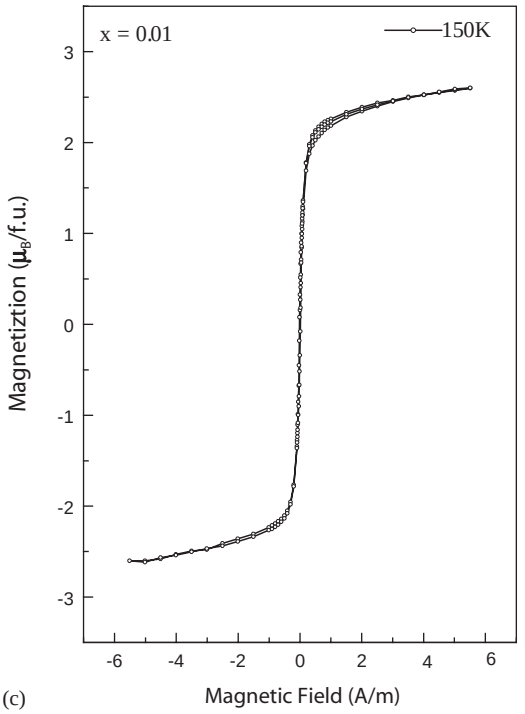
x = 0.01
150K
Magnetiztion (μB/f.u.)
Magnetic Field (A/m)

(c)

regions. It is probable that low field loop arises from conversion of predominantly C- to FM- and high field loop from predominantly A- to FM-type magnetic order.

7. Conclusion

We have shown that the change in field-induced metastability and metal–insulator transition on chromium substitution in $Nd_{0.5}Sr_{0.5}MnO_3$ arises due to change in the small polaron stabilization energy, ε_p, and the number of the charge carrier in the low temperature antiferromagnetic insulating state. The temperature dependence of resistivity is accounted on the basis of correlated polaron transport mechanism including electron–phonon and spin–spin scattering processes in the ferromagnetic metal, antiferromagnetic and paramagnetic insulating phases. In the low temperature antiferromagnetic region with and without charge order a single controlling parameter, the number of charge carriers, is found to account for the large variation in resistivity. The origin of metastability in the chromium substituted $Nd_{0.5}Sr_{0.5}MnO_3$ has been attributed to the simultaneous presence of regions of C-, A- and FM-type magnetic order whose volume fraction depends on the chromium concentration, temperature and the external field.

Acknowledgements

We are thankful to Department of Science and Technology, Government of India for the financial support.

References

[1] Y. Tokura, Y. Tomioka, H. Kuwahara, A. Asamitsu, Y. Moritomo, M. Kasai, J. Appl. Phys. 79 (1996) 5288.
[2] H. Kuwahara, Y. Tomioka, A. Asamitsu, Y. Moritomo, Y. Tokura, Science 270 (1995) 961.
[3] A. Biswas, A.K. Raychaudhuri, R. Mahendiran, A. Guha, R. Mahesh, C.N.R. Rao, J. Phys.: Condens. Matter 9 (1997) L355.
[4] R. Mahendiran, M.R. Ibarra, A. Maignan, F. Millange, A. Arulraj, R. Mahesh, B. Raveau, C.N.R. Rao, Phys. Rev. Lett. 82 (1999) 2191.
[5] P.W. Woodword, D.E. Cox, T. Vogt, C.N.R. Rao, A.K. Cheetan, Chem. Mater. 11 (1999) 358.
[6] R. Kajimoto, H. Yoshizawa, H. Kawano, H. Kuwahara, Y. Tokura, Phys. Rev. B 60 (1999) 9506.
[7] C. Ritter, R. Mahendiran, M.R. Ibarra, L. Morellon, A. Maignan, B. Raveau, C.N.R. Rao, Phys. Rev. B 61 (2000) R9229.
[8] A.S. Carneiro, F.C. Fonseca, R.F. Jardim, T. Kimura, J. Appl. Phys. 93 (2003) 8074.
[9] T. Kimura, Y. Tomioka, R. Kumai, Y. Okimoto, Y. Tokura, Phys. Rev. Lett. 83 (1999) 3940.
[10] A. Biswas, A. Arulraj, A.K. Raychaudhari, C.N.R. Rao, J. Phys.: Condens. Matter 12 (2000) L101;
P.V. Vanitha, R.S. Singh, S. Natarajan, C.N.R. Rao, Solid State Commun. 109 (1999) 135.
[11] P.G. de Gennes, Phys. Rev. 118 (1960) 141.
[12] C.M. Srivastava, J. Phys.: Condens. Matter 11 (1999) 4539.
[13] T. Hayashi, N. Miura, Y. Tomioka, Y. Tokura, J. Phys. Chem. Solids 63 (2002) 925.
[14] E.J.W. Verwey, Nature 144 (1939) 327.
[15] J.B. Goodenough, The Verwey Transition, in: C.M. Srivastava (Ed.), Recent Advances in Materials Research, Oxford and IBH Publishing Co., 1984, p. 3;
V.A.M. Brabers, et al., Ferrites, in: Proceedings of the 8th International Conference on Ferrites ICF8, Kyoto and Tokyo, Japan, 2000, p. 123;
V.A.M. Brabers, et al., PRB 58 (1998) 14163;
V.A.M. Brabers, et al., Physica B 266 (1999) 321;
C.M. Srivastava, et al., J. Magn. Soc. Japan 22 (Suppl. No S1) (1998) 15.
[16] H.G. Reik, in: J.T. Devreese (Ed.), Polarons in Ionic Crystals and Polar Semiconductors, North-Holland, Amsterdam, 1972, pp. 679–714.
[17] N. Kallel, J. Dhahri, S. Zemni, E. Dhahri, M. Oumezzine, M. Ghedira, H. Vincent, Phys. Stat. Sol. (A) 184 (2001) 319.
[18] P.W. Anderson, H. Hasegawa, Phys. Rev. 100 (1955) 675.
[19] H. Kawano, R. Kajimoto, H. Yoshizawa, Y. Tomioka, H. Kuwahara, Y. Tokura, Phys. Rev. Lett. 78 (1997) 4253.
[20] J.B. Goodenough, Phys. Rev. 100 (1955) 564.
[21] M.V. Zimmermann, C.S. Nelson, J.P. Hill, R. Doon Gibbs, M. Blume, D. Casa, B. Keimer, Y. Murakami, C.-C. Kao, C. Venkataraman et al., J. Magn. Magn. Mater. 233 (2001) 31.
[22] R. Mahendiran, M. Hervieu, A. Maignan, C. Martin, B. Raveau, Solid State Commun. 114 (2000) 429.
[23] M.A. Manekar, S. Chaudhary, M.K. Chattopadhyay, K.J. Singh, S.B. Roy, P. Chaddah, Phys. Rev. B 64 (2001) 104416;
K.J. Singh, S. Chaudhary, M.K. Chattopadhyay, M.A. Manekar, S.B. Roy, P. Chaddah, Phys. Rev. B 65 (2002) 09419;
M. Manekar, S. Choudhary, M.K. Chatopadhyay, K.J. Singh, S.B. Roy, P. Chaddah, J. Phys.: Condens. Matter 14 (2002) 4477.